

# Topology near the transition temperature in lattice gluodynamics analyzed by low lying modes of the overlap Dirac operator

E.-M. Ilgenfritz

*Joint Institute for Nuclear Research, VBLHEP, 141980 Dubna, Russia*

B. V. Martemyanov

*Institute of Theoretical and Experimental Physics, 117259 Moscow, Russia*

*National Research Nuclear University MEPhI, 115409, Moscow, Russia*

*Moscow Institute of Physics and Technology, 141700, Dolgoprudny, Moscow Region, Russia*

M. Müller-Preussker

*Humboldt-Universität zu Berlin, Institut für Physik, 12489 Berlin, Germany*

(Dated: February 3, 2014)

Topological objects of  $SU(3)$  gluodynamics are studied at the infrared scale near the transition temperature with the help of zero and near-zero modes of the overlap Dirac operator. We construct UV filtered topological charge densities corresponding to three versions of the temporal boundary condition applied to this operator, for which the zero mode is known to be located on corresponding three constituent dyons (antidions) in the reference case of an analytical (anti)caloron solution. The clustering of the three topological charge densities marks the positions of three types of dyons and antidions which can therefore be considered as present in equilibrium (Monte Carlo) gluonic fields at the given resolution scale. We classify them either as constituents of nondissociated (anti)calorons or as constituents of (anti)dion pairs or as isolated (anti)dyons. The pattern of the Polyakov loop describing the centers and the interior of these clusters is observed after a limited number of overimproved cooling steps and resembles the description known from analytical caloron solutions.

PACS numbers: 11.15.Ha, 12.38.Gc, 12.38.Aw

Keywords: Lattice gauge theory, overlap Dirac operator, caloron, dyon

## I. INTRODUCTION

Two basic properties of QCD are confinement (of quarks and gluons) and the spontaneous breaking of chiral symmetry at low temperature and density. Both properties are believed to be intimately connected with each other and to originate from a certain complex structure of the QCD vacuum state, the simplest manifestations of which being condensates of gluon and quark fields. The field fluctuations contributing to these condensates are, however, space-time and scale dependent. One of the aims of Lattice Gauge Theory is to reveal the corresponding structures. One school of thought claims that - at the infrared scale - the origin of both mechanisms can be traced back to semiclassical objects of QCD. Until the late 1990's lattice studies tried to figure out the "instanton structure" of the vacuum by "cooling" or "smearing", the role of which today is taken by the Wilson flow [1, 2]. The number of cooling steps was providing the running scale of resolution [3]. For reviews of the instanton picture itself we refer to the reports [4, 5]. Then, including a slight extension to non-zero temperature  $T$ , more general semiclassical objects, Kraan-van Baal-Lee-Lu (KvBLL) calorons [6–8], have replaced instantons as the carriers of topological charge, with new features like a variable asymptotic holonomy and (topologically) fractionally charged constituents (dyons). Still,

KvBLL calorons have not reached that level of familiarity that instantons have enjoyed among lattice practitioners. Today it is folklore to say that the instanton gas is able to explain chiral symmetry breaking while it fails to provide a mechanism for confinement. Constituent dyons, however, when considered as rarefied gas without interaction or with Coulomb-like interaction, give confining behavior for space-like Wilson loops and for correlators of Polyakov loops. The history of this idea ranges from the 70's to the recent past [9–13].

Therefore, it is of some interest to search for dyons in standard Monte Carlo configurations, representing lattice gauge fields at different temperatures, in order to assess the reality of these models. For the purpose of this investigation, the fermion eigenmodes of a chirally (almost) perfect Dirac operator (i. e. the massless overlap operator) are promising to be an adequate tool. In this paper we shall employ this tool to pure  $SU(3)$  gauge theory. We stress that a cutoff with respect to the eigenvalues plays the role of the running scale. This interpretation has been given to the cutoff already in previous applications of the overlap operator [14] for investigations of topological structure at  $T = 0$ . In the context of finite temperature the splitting of calorons into dyons is a phenomenon worth to study. Then the choice of the temporal boundary condition (b.c.) applied to the analysing Dirac operator is an additional free parameter allowing to

separate different degrees of freedom inside a caloron (dyon constituents) according to their inherent holonomy.

The caloron with nontrivial holonomy [6–8] has the remarkable property that the single zero mode of the Dirac operator locates on different constituent dyons [15, 16], depending on the temporal b.c. applied to the Dirac operator. In lattice simulations, the change of zero mode localization with the change of b.c. was observed for thermal configurations of lattice gauge fields [17, 18]. In the case of  $SU(2)$  lattice gauge theory it has been seen that this property is shared also by near-zero modes [19, 20]. Thus, the low lying modes of the overlap Dirac operator can be used as an effective tool to detect distinct topological objects at a corresponding scale directly within Monte Carlo configurations of lattice gauge fields (without cooling or smearing).

The angle characterizing the b.c. needs to be varied in order to detect really *all sorts of dyons* by the fermionic method. Only this allows to check the phenomenological relevance of the KvBLL caloron picture which is assumed in models like those mentioned above. In  $SU(3)$  lattice gauge theory, the properties of constituent dyons have been studied thoroughly earlier in cooled (i. e. classical) configurations of lattice gauge fields [21]. The interrelation between localization and delocalization (in space-time position and with respect to extension) and the angle of the b.c. of the fermion field was demonstrated in detail. The phenomenological relevance of the dyon picture, however, was not yet in the scope of that work.

To carry over the method of analysis, developed previously for the  $SU(2)$  case in Refs. [19, 20, 22], to the case of  $SU(3)$  gauge fields is not trivial. Having three (and among them, two independent) eigenphases of each local holonomy, enforces to consider the complex plane of the Polyakov loop and to introduce an angle modifying the b.c. beyond the antiperiodic and periodic case. Our aim is to classify, according to the KvBLL caloron picture (outlined in the Appendix), topological objects in field ensembles of pure  $SU(3)$  gluodynamics, generated close to the deconfinement transition temperature, with the help of zero and near-zero modes of the overlap Dirac operator, modified by different temporal boundary conditions.

Our previous study of topological objects at non-zero temperature in  $SU(2)$  lattice fields, based on smearing [22, 23] or on an overlap fermion analysis [19, 20], has resulted in the following picture of the topological content of  $SU(2)$  gauge theory. At low temperatures, the relevant topological objects are nondissociated calorons with maximally nontrivial holonomy. With increasing temperature, their composite nature becomes recognizable as the dissociation into two dyons (i. e. selfdual non-Abelian) monopoles of topological charge  $\pm 1/2$ . Approaching the critical temperature  $T_c$  (of the deconfining phase transition),

approximately half of the calorons have become dissociated, retaining the symmetry of the two dyons. Above the critical temperature a non-zero expectation value of the averaged Polyakov loop  $\langle L \rangle$  develops. This results in an asymmetry between the dyons: light dyons (with the local Polyakov loop of same sign as  $\langle L \rangle$ ) become the most abundant topological objects, while heavy dyons (and, even more so, nondissociated calorons) are suppressed. In the present paper we will see to what extent this picture translates to the three dyons per caloron of  $SU(3)$  gauge theory, which would be distinguished – by analogy – by the phase of the complex-valued Polyakov loop.

In Section II the generation of the two lattice ensembles characterizing temperatures slightly above and below the deconfining transition is described. In Section III the dependence of the eigenvalue spectrum of the overlap operator on the observed physical phase *and on the boundary condition* is demonstrated. We sketch the fermionic construction of the topological charge density, restricted to the infrared scale by the cutoff, with the help of the eigenmodes for three different fermionic boundary conditions. Finally, the results of a cluster analysis of these densities is presented with respect to the formation of clusters (“dyons”) of different local holonomy and of “bound states” of different type dyons (including complete calorons). Section IV raises the question to what extent the fermionic topological density (if averaged over the three different b.c.’s in order to include all types of dyons) can be reproduced by cooling techniques. An optimal number of cooling steps is found which solves this problem in an impressive way. With this amount of cooling, it becomes possible to understand the systematics of the Polyakov loop in different single dyons and to understand the scatter plot of the Polyakov loop inside bigger clusters (representing dyon pairs and calorons). In Section V we conclude that the resolution chosen for this investigation supports the idea that semiclassical objects of dyon type characterize the topological structure at this scale. The Appendix is devoted to a brief summary of those aspects of calorons that have been essential for this study.

## II. SETUP OF THE INVESTIGATION

The  $SU(3)$  gauge field configurations for this investigation have been generated on a lattice of size  $20^3 \times 6$  by sampling the pure  $SU(3)$  gauge theory using the Lüscher-Weisz action [24]. Improved gauge actions are known to be mandatory for analyses using the overlap Dirac operator, in order to take full advantage of their good chiral properties. The sampled gauge fields are smoother than those sampled with the Wilson action. In particular, the idea of our analysis rests on the observation that changing the boundary condition leaves the number of zero modes unchanged.

The Lüscher-Weisz action has also been used in the QCDSF topological studies [14] of pure Yang-Mills theory with overlap fermions and by Gattringer and coworkers [25, 26] when they were using a specific chirally improved fermion action for topological investigations. In the  $SU(2)$  case, the tadpole-improved Symanzik action has been applied for analogous reasons in our previous work [19, 20, 27].

In addition to the plaquette term (pl), the Lüscher-Weisz action includes a sum over all  $2 \times 1$  rectangles (rt) and a sum over all parallelograms (pg), i.e. all possible closed loops of length 6 along the edges of all 3-cubes

$$S[U] = \beta \left( \sum_{pl} \frac{1}{3} \text{Re Tr}[1 - U_{pl}] + c_1 \sum_{rt} \frac{1}{3} \text{Re Tr}[1 - U_{rt}] + c_2 \sum_{pg} \frac{1}{3} \text{Re Tr}[1 - U_{pg}] \right), \quad (1)$$

where  $\beta$  is the principal inverse coupling parameter, while the coefficients  $c_1$  and  $c_2$  are computed using results of one-loop perturbation theory and tadpole improvement [28–30]:

$$c_1 = -\frac{1}{20u_0^2}[1 + 0.4805\alpha], \quad c_2 = -\frac{1}{u_0^2}0.03325\alpha. \quad (2)$$

For a given  $\beta$ , the tadpole factor  $u_0$  and the lattice coupling constant  $\alpha$  are self-consistently determined in terms of the average plaquette

$$u_0 = \left( \langle \frac{1}{3} \text{Re Tr } U_{pl} \rangle \right)^{1/4}, \quad \alpha = -\frac{\ln \left( \langle \frac{1}{3} \text{Re Tr } U_{pl} \rangle \right)}{3.06839} \quad (3)$$

in the course of a series of iterations.

Two ensembles, each consisting of 50 configurations, have been generated for the overlap analysis with values of the principal inverse coupling values  $\beta = 8.20$  and  $\beta = 8.25$ . For the generation of these configurations 1500 empty sweeps have been performed in between in order to make the configurations uncorrelated among each other. According to previous work [31], these ensembles correspond to temperatures close to the phase transition point  $\beta = \beta_c$ .

By lowering  $\beta$  we have tried to look deeper into the confining phase in order to find more signatures for caloron dominance (with equally weighted constituent dyons related to maximally non-trivial holonomy). However, as mentioned above, the proper applicability of the overlap operator diagonalization is limited to a range of sufficiently large  $\beta$ -values (i. e. to sufficiently smooth lattice gauge fields) even if the Lüscher-Weisz action is in use. This closeness to  $\beta_c$  had to be accepted as necessary condition in the confining phase in order to ensure that the number of

zero-modes (the “topological index”) of a given gauge field will not change with the choice of boundary condition for the fermion field.

In order to characterize the two ensembles, we present in Fig. 1a the distributions of the real part of the spatially averaged Polyakov loop  $Re(L)$  (without any smearing or cooling) rotated to the real  $Z_3$  sector  $-\pi/3 < \arg(L) < \pi/3$ . A global  $Z_3$  rotation has been applied whenever  $L$  was found with  $\pi/3 < \arg(L) < \pi$  or  $-\pi/3 > \arg(L) > -\pi$ . The distributions have been obtained from 15000 subsequent Monte Carlo configurations. They were sampled independently from the configurations that have been used in the overlap analysis later on. We show the analogous comparison for the distributions of the modulus of the spatially averaged Polyakov loop  $|L|$  in Fig. 1b. Both kinds of distributions suggest that configurations obtained at  $\beta = 8.20$  belong mainly to the confining phase (with an admixture from the deconfining phase), and that the configurations at  $\beta = 8.25$  refer exclusively to the deconfining phase.

### III. TOPOLOGICAL CLUSTERS

We have analyzed the configurations of the two ensembles by identifying and investigating in each case  $N = 20$  near-zero eigenmodes of the overlap Dirac operator. Its realization is an  $SU(3)$  extension of the  $SU(2)$  overlap Dirac operator described in [19]. Originally, the choice of  $N = 20$  modes was mainly dictated by the limited amount of workstation resources for this long-term project. As described later, the resulting analyzing power happened to be tantamount to approximately 20 overimproved cooling steps. The spectral analysis has been performed for three temporal b.c.’s applied to the fermion field  $\psi$ , for which – in the case of a single-caloron solution with maximally nontrivial holonomy – the zero mode of the fermion field is maximally localized at one of its three constituent dyons (see Appendix):

$$\psi(1/T) = \exp(i\phi)\psi(0) \quad (4)$$

with

$$\phi = \begin{cases} \phi_1 \equiv -\pi/3, \\ \phi_2 \equiv +\pi/3, \\ \phi_3 \equiv \pi. \end{cases} \quad (5)$$

For each of these b.c.’s we have determined the topological index and have checked that it was obtained – in the  $\beta$  range under consideration – independent of the choice of  $\phi$ .

The corresponding spectra of the 20 near-zero eigenmodes are shown in Fig. 2 for two configurations representative for  $\beta = 8.20$  and  $\beta = 8.25$ , respectively. In the confinement case (a) these spectra have a nonzero

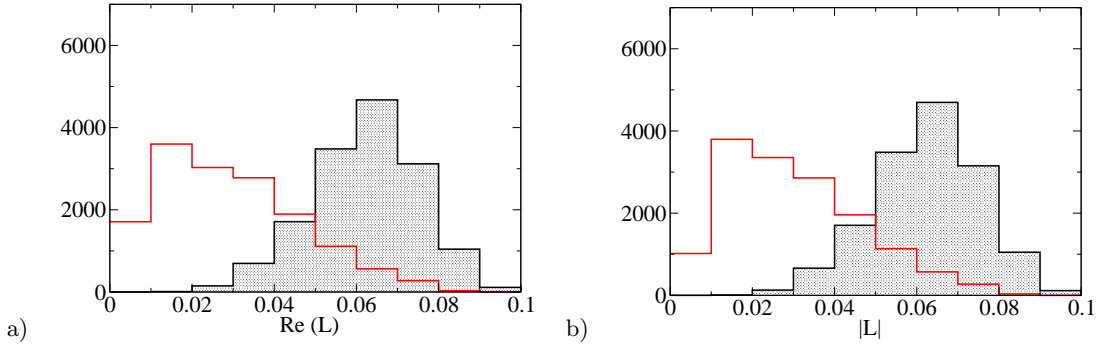


FIG. 1: The distributions a) of the real part of the spatially averaged Polyakov loop  $Re(L)$  (eventually rotated to the real  $Z_3$  sector) and b) of the modulus  $|L|$ , both at  $\beta = 8.20$  (red curve) and  $\beta = 8.25$  (shadowed), each based on a statistics of 15000 configurations.

density around zero value (signalling spontaneous violation of chiral symmetry); in the deconfinement case (b) a gap in the spectra is appearing. Notice for the latter case the occurrence of an even larger gap width for the third (i.e. antiperiodic) boundary condition ( $\phi_3$ ). The spatially averaged Polyakov loop  $L$  for this configuration has fallen into the real  $Z_3$  sector  $-\pi/3 < \arg(L) < \pi/3$ . The observation of the gap is in agreement with results of earlier studies [32] using the chirally improved Dirac operator. In order to proceed further, we have reconstructed from the zero and the non-zero modes the profiles of the UV-filtered topological charge density according to its spectral representation (for details see [14, 33])

$$q_{i,N}(x) = - \sum_{j=1}^N \left( 1 - \frac{\lambda_{i,j}}{2} \right) \psi_{i,j}^\dagger(x) \gamma_5 \psi_{i,j}(x), \quad (6)$$

where  $j$  enumerates the eigenvalues  $\lambda_{i,j}$  equal and closest to zero. These eigenvalues  $\lambda_{i,j}$ , as well as the corresponding modes  $\psi_{i,j}(x)$ , are also characterized by the  $i$ -th boundary condition. Correspondingly, the UV-filtered topological density  $q_{i,N}(x)$  depends on the boundary condition, too.

We have applied a cluster analysis with a variable lower cut-off  $q_{\text{cut}} > 0$  to these density functions. In a first step the algorithm identifies the interior of all clusters (“topological cluster matter”) as the region where  $|q(x)| > q_{\text{cut}}$ . The crucial next step is to enquire the connectedness between the lattice points in order to form individual clusters out of this “cluster matter”. Neighbouring points with  $|q(x)|$  above threshold and sharing the sign of topological density are said to form the same cluster. The cut-off  $q_{\text{cut}}$  has been chosen such as to resolve the given continuous distribution into a maximal number of internally connected while mutually separated clusters. The cut-off value has been independently adapted for each configuration. The purpose of the cluster analysis was to dis-

cover extended objects that we are going to consider as dyon candidates.

For the lower temperature ( $\beta = 8.20$ ) we have found the following average numbers of clusters per configuration comprising all 50 configurations and corresponding to the boundary conditions  $i = 1, 2, 3$ :

$$N_1 = 18.4(0.4), \quad N_2 = 18.6(0.5), \quad N_3 = 16.6(0.3).$$

These numbers (and also the following ones) are ordered in a way which corresponds to spatially averaged Polyakov loop values  $L$  globally rotated into the real  $Z(3)$  sector  $-\pi/3 < \arg(L) < \pi/3$ .  $N_1$  and  $N_2$  are coinciding within errors (the latter given in parentheses), while  $N_3$  is slightly lower. The average size of all clusters amounts to 146 lattice points. That in the confining phase the abundance of all three types of clusters is roughly equal can be interpreted in terms of dyons with maximally nontrivial holonomy (see Appendix). Assuming the lattice scale fixed by the transition temperature for  $SU(3)$  gluodynamics,  $T_c = 300$  MeV [31] we obtain the physical dyon cluster density. It is equal to  $6 \text{ fm}^{-4}$  and corresponds to the presented above  $50 \cdot (N_1 + N_2 + N_3)$  clusters.

Since we observe a slight asymmetry  $N_3 < N_1 = N_2$  pointing to an admixture of configurations related to deconfinement we have applied a cut for the modulus  $|L| < 0.3$  (fixed after improved cooling according to the description given in the following section). We find from the 23 configurations surviving this cut the average numbers per configuration

$$N_1 = 17.8(0.6), \quad N_2 = 18.3(0.6), \quad N_3 = 17.2(0.5).$$

These numbers overlap within errors as expected in the confinement case.

The inverse participation ratios (IPR) calculated from the zero modes (see Refs. [14, 34, 35]) for three types of b.c.’s turn out to be

$$IPR_1 = 6.8(0.8), \quad IPR_2 = 6.4(1.0), \quad IPR_3 = 15.2(1.7),$$

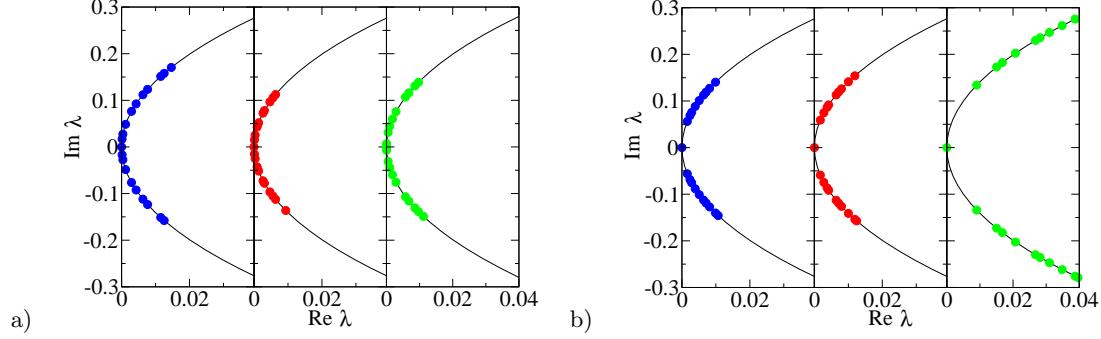


FIG. 2: For two typical configurations and in each case for the three versions of the fermion temporal b.c. (according to Eqs. (4, 5)) the 20 lowest eigenvalues of the  $SU(3)$  overlap Dirac operator are shown, for a)  $\beta = 8.20$  and b)  $\beta = 8.25$ , respectively. In both of the panels for  $\phi = \phi_1$  the spectrum is shown left (in blue), for  $\phi = \phi_2$  in the middle (in red), and for  $\phi = \phi_3$  (antiperiodic b.c.) it is plotted right (in green), respectively.

where the statistical errors are given in parentheses. Having applied the above mentioned cut for  $|L|$  we find

$$IPR_1 = 5.8(0.9), \quad IPR_2 = 5.0(0.6), \quad IPR_3 = 8.5(0.6).$$

With the cut taken into account the asymmetry is much less pronounced but still there. Having the properties of calorons and their constituents in mind (see the last paragraphs of the Appendix) we interpret this finding as a stronger localization of those dyons getting a larger mass when approaching the transition temperature from below or moving into the deconfinement phase. Those heavier constituents are expected to be statistically suppressed, which seems to be already visible, because  $N_3$  is a bit lower than  $N_1$  and  $N_2$ .

Next we have checked whether clusters of different type appeared correlated among each other. We found at the lower temperature (not applying any cut)

$$\begin{aligned} \text{number of isolated clusters} &= 1299 & (49\%), \\ \text{number of clusters in pairs} &= 782 & (29\%), \\ \text{number of clusters in triplets} &= 597 & (22\%), \end{aligned}$$

where the clusters of different type are counted as connected in pairs or triplets if the distance was less than two lattice spacings. Interpreted in terms of calorons of non-trivial holonomy this means that we see full caloron-like clusters consisting of three constituents on one hand and also completely dissolved caloron constituents on the other hand.

For the higher temperature ( $\beta = 8.25$ ) we have found the following numbers of clusters per configuration (on all 50 configurations) corresponding to the b.c.'s  $i = 1, 2, 3$ :

$$N_1 = 20.7(0.6), \quad N_2 = 20.6(0.6), \quad N_3 = 17.1(0.4).$$

The average size of these clusters amounts to 172 lattice points. The density of clusters is higher than at lower temperature:  $8 \text{ fm}^{-4}$ . In this ensemble we find already a fully developed asymmetry of the distribution of the spatially averaged Polyakov loop  $L$ . Corresponding to that, applying the antiperiodic b.c. to the Dirac operator leads to a lower number  $N_3$  of clusters of the topological density. Under these circumstances given by the ensemble average Polyakov loop (i. e. the asymptotic holonomy for a would-be exact caloron) the type of dyons corresponding to the antiperiodic boundary condition acquires a higher action (see Appendix). Thus, one could have expected them to be suppressed in the equilibrium ensemble. A pronounced asymmetry between the different b.c.'s is seen also in the inverse participation ratios that the zero modes acquire:

$$IPR_1 = 7.9(0.8), \quad IPR_2 = 7.2(0.7), \quad IPR_3 = 24.6(1.8).$$

In other words, the zero modes sitting on “heavy dyons” (that we found as clusters of the topological density defined by the antiperiodic b.c.) are localized about three times as much than the zero modes sitting on “light dyons” (detected using the other two b.c.'s).

Above the deconfinement temperature ( $\beta = 8.25$ ) we studied also the correlation properties of clusters of different type and found them organized as follows:

$$\begin{aligned} \text{number of isolated clusters} &= 1600 & (55\%), \\ \text{number of clusters in pairs} &= 834 & (28\%), \\ \text{number of clusters in triplets} &= 492 & (17\%). \end{aligned}$$

One can conclude that at the temperature above the phase transition the amount of fully dissociated dyons has much grown relative to the lower temperature at the expense of dyons enclosed in clusters of three dyons (i.e. complete calorons).

#### IV. POLYAKOV LOOP PORTRAITS OF TOPOLOGICAL CLUSTERS

In order to provide evidence for the nature of the clusters as dyons (caloron constituents) the profile of the local Polyakov loop inside them should be monitored. It is known that some amount of gauge field cooling must be applied to see emerging patterns of the Polyakov loop. We have used here (as already before) overimproved cooling [36]. This variant of cooling has been found to successfully characterize the gauge field configurations according to their total topological charge if it is continued to the final (self-dual or anti-selfdual) plateaux [37]. Here, however, we have restricted ourselves to the first steps of overimproved cooling. More precisely, we decided for each gauge field configuration individually to cool down to the cooling step, when the UV-filtered topological charge density of uncooled configurations – built on the overlap modes and averaged over the boundary conditions – is optimally fitted by the gluonic topological charge density of the corresponding cooled configuration [38–40]. [44] The result of this comparison has lead us to the conclusion that after  $\approx 20$  cooling steps a gluonic topological density can be found that approaches best the UV-filtered overlap topological density (based on 20 modes per configuration). The quality of the agreement is demonstrated in Fig. 3 for typical configurations found for  $\beta = 8.20$  (left panel) and for  $\beta = 8.25$  (right panel). The characteristic peak structure found along lines of subsequent lattice sites (periodically penetrating the lattice several times with a minimal off-set) is reproduced by both (fermionic and gluonic) methods. In the average the agreement turned out to be a bit better for the confinement case ( $\beta = 8.20$ ) than for deconfinement one ( $\beta = 8.25$ ). Closely related to this, for 90% (85%) of the configurations obtained at  $\beta = 8.20$  ( $\beta = 8.25$ ) we observed the total gluonic topological charge measured after cooling to be equal to the topological charge assigned by the number of zero modes of the overlap Dirac operator without any cooling, i. e. in accordance with the index theorem. We should recall that – for our choice of the gauge action and sufficiently high  $\beta$ -values – the index was found independent of the chosen fermionic boundary condition.

With the cooling steps the local pattern of the Polyakov loop (once it has become discernible from the noise) is smoothed [37]. A related effect is reported in Fig. 4, where the scatter plots of the *spatially averaged* Polyakov loop  $L$  before and after cooling are shown for a)  $\beta = 8.20$  and b)  $\beta = 8.25$ , respectively. For  $\beta = 8.20$  (confinement) the initial distribution around the origin expands more or less isotropically, while in the corresponding scatter plot for  $\beta = 8.25$  (deconfinement) the spatially averaged Polyakov loop  $L$  is driven by cooling toward the three “corners” rep-

resenting trivial holonomy.

From the study of classical calorons and their dyon structure [21] we know that the “center of the dyon”, is characterized by a minimal distance between two almost-degenerate eigenphases of the local holonomy.

Having carried out the optimal number of cooling steps (see above) the local Polyakov loop – in the following denoted ‘ $PL$ ’ – measured at the *center of each cluster* (corresponding to b.c.’s of type  $i = 1, 2$  and 3 and to spatially averaged Polyakov loop values  $L$  rotated into the real  $Z(3)$  sector  $-\pi/3 < \arg(L) < \pi/3$ ) for  $\beta = 8.20$  (confinement) has been put into the scatter plots shown in Fig. 5. The dyonic nature of the clusters would be underlined by the correlation between the temporal b.c. applied to the  $SU(3)$  overlap Dirac operator (selecting one sort of dyons showing up in the cluster analysis) and the values of the local Polyakov loop in the center of the corresponding topological clusters. What is actually seen in Figs. 5a, b and c is a statistical preference of coincidences of two holonomy eigenvalues. The scatter plots are relatively concentrated along the appropriate sides of the Polyakov triangle (where two eigenphases collide). This happens on the side pointing towards the respective angle  $\phi$ . Having in mind that some of the configurations can be related to deconfinement we have applied the cut  $|L| < 0.3$  also for this case. The corresponding modified result is shown in Fig. 6. We see the clustering at the corners of the Polyakov triangle has disappeared.

For  $T \gtrsim T_c$ , at  $\beta = 8.25$ , the initially small rotational asymmetry in the distribution of the spatially averaged Polyakov loop  $L$  becomes strongly amplified in the course of cooling in the direction of trivial holonomy (see Fig. 4b). One sees also the small admixture of other (non-real)  $Z_3$  sectors (which was intentionally hidden by the  $Z(3)$  rotation in Fig. 1a). The pattern of the local Polyakov loop  $PL$  in the centers of the clusters is distorted correspondingly, in contrast to the confinement phase, as it is shown in Fig. 7. Now the scatter plots in Fig. 7a and b are concentrated closer to  $PL = +1$ , i. e. to the real corner of the Polyakov triangle pointing to trivial holonomy. This is what one would expect from the discussion of KvBLL solutions at the end of the Appendix (see Fig. 9). Having a central value  $L \simeq +1$  means that those dyons observed with b.c.’s  $\phi_1$  and  $\phi_2$  should have small masses  $m_1, m_2$  and positions in the Polyakov triangle at the upper and lower border lines, respectively, close to the corner  $PL = +1$ . On the contrary, for antiperiodic b.c. ( $\phi_3 = \pi$ ) we would expect to observe dyons with large mass  $m_3$  and positions at the border line opposite to  $PL = +1$ . Such objects are really seen in Fig. 7c but only as a minor fraction. That these heavy objects should be statistically suppressed was expected from the lowered number  $N_3$  in the previous section but not as dramatically as it is seen here from those points. The majority of clusters in this figure

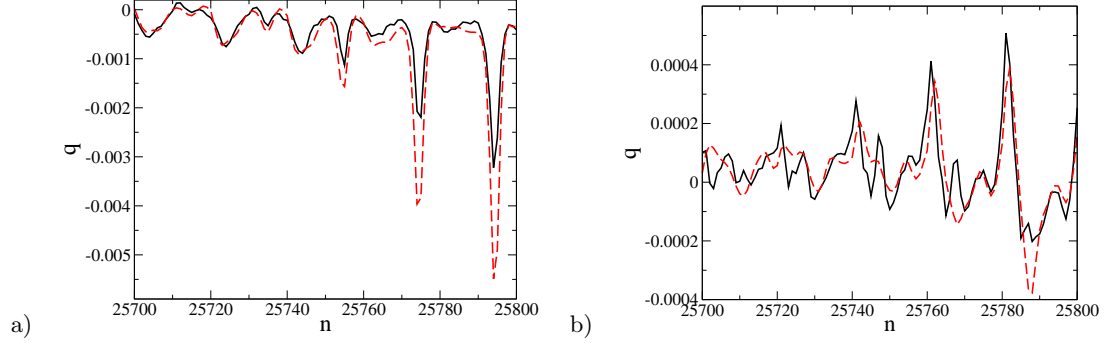


FIG. 3: Comparison (along some string of lattice sites) of the overlap topological charge density of a typical configuration for a)  $\beta = 8.20$  and b)  $\beta = 8.25$  (averaged over b.c.'s, shown as solid black line) with the gluonic topological charge density (dashed red line). The latter is determined after an optimal number of overimproved cooling steps (see text).

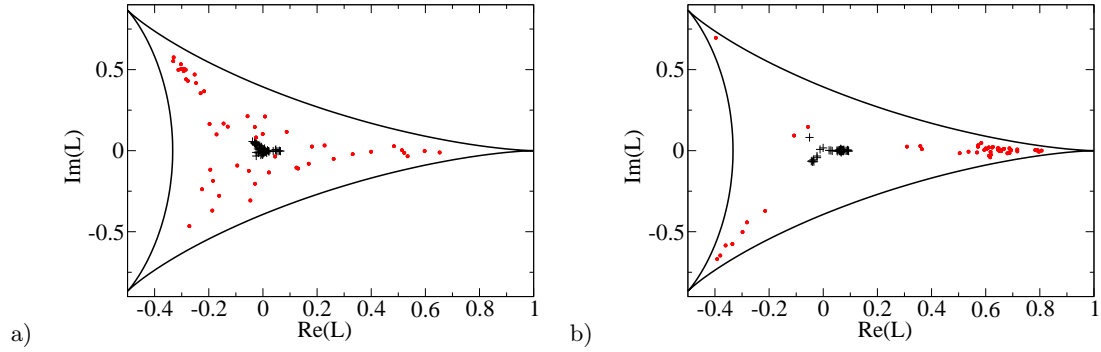


FIG. 4: Scatter plots of the spatially averaged Polyakov loop  $L$  before (black crosses) and after cooling (red dots) for a)  $\beta = 8.20$  and b)  $\beta = 8.25$ , respectively.

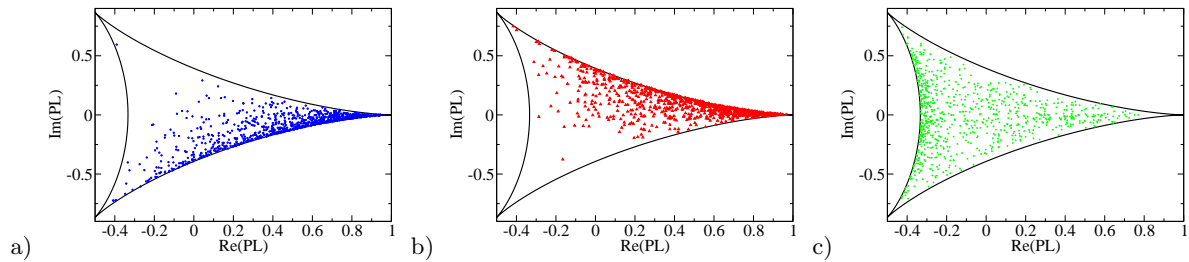


FIG. 5: For three cases of the fermion temporal b.c., the zero and near-zero modes of  $SU(3)$  overlap Dirac operator define three different profiles of the topological charge density on a configuration belonging to the ensemble at  $\beta = 8.20$  ( $T \simeq T_c$ ). Each cluster of these profiles is represented in the plots by the Polyakov loop  $PL$  measured in its cluster center. The ordering corresponds to spatially averaged Polyakov loop rotated into the real  $Z(3)$  sector (after improved cooling). a) 918 clusters of first type (blue), b) 929 clusters of second type (red), c) 831 clusters of third type (green).

are covering points closer to  $PL = +1$ . They cannot be explained from caloron structures with three constituents each. One may speculate that they also correspond to (anti)dyons but with some intermediate

mass value. However, we cannot exclude that they are topological fluctuations, which cannot be interpreted in terms of dyons. They might be also “dislocations” corresponding to some mismatch of the Polyakov loop



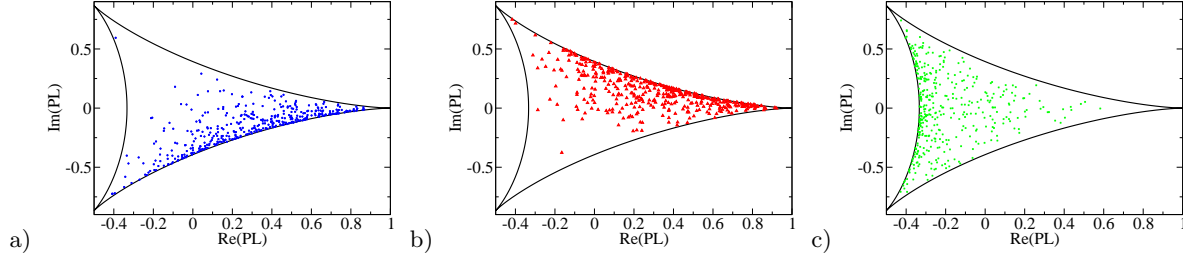


FIG. 6: Same as in Fig. 5 but with a cut  $|L| < 0.3$  (after improved cooling) leading to 23 (out of 50) configurations. a) 409 clusters of first type (blue), b) 421 clusters of second type (red), c) 395 clusters of third type (green).

obtained after improved cooling and the topological clusters seen from a finite number of fermion modes.

Finally, for both cases  $\beta = 8.20$  and  $\beta = 8.25$ , respectively we have searched for “clouds” of topological charge which are either

- bigger “clouds” formed when three dyons of different type are close to each other (forming a triplet of clusters = calorons), or
- bigger “clouds” formed when two dyons of different type are close to each other (forming three types of cluster pairs), or
- “clouds” consisting of isolated dyons (existing in three types).

Scanning the local Polyakov loop point by point, we are presenting here examples as scatter plots in Figs. 8a, b, c drawn for the confinement situation ( $\beta = 8.20$ ). The number of points shown corresponds to the actual number of lattice points forming the respective example of a topological “cloud”. These distributions of points in the complex plane of the Polyakov loop qualitatively follow the pattern expected for analytical calorons [21, 41] with their dyonic structure. However, this feature is found only in the confining phase, whereas in the deconfinement phase the third type of “clouds” (isolated dyons and possible “dislocations”) turn out to be dominant.

## V. CONCLUSIONS

In  $SU(3)$  lattice gauge theory, using a small number of modes of the overlap Dirac operator with eigenvalues closest to zero, we have investigated clusters formed by the (fermionic) topological charge density, appearing in association with three different types of boundary conditions that have been applied to the fermion field.

Assuming that these clusters correspond to dyons, we have demonstrated how their frequency of occurrence and the tendency to combine into triplets

(calorons) or to form pairs of dyons or to remain isolated depends on the temperature. An increasing caloron dissociation is observed as the result of the small temperature increase across the phase transition.

It turned out that the angle  $\phi$  entering the boundary condition has no absolute meaning. Instead, the angle only relative to the phase of the average Polyakov loop gives a unique definition of heavy and light dyons in the deconfined phase. Heavy dyons are selected by  $\phi$  chosen opposite to the phase of the average Polyakov loop. Taking the phase of the average Polyakov loop into account also in the confined phase does not change the approximate equality of numbers of dyons of different type, but it sharpens the relation between the distribution of dyons in the complex Polyakov loop plane on one hand and the applied boundary condition. In other words, for confinement and deconfinement a unique relation between  $\phi$  and the positioning of the corresponding dyon clusters in the complex plane of the local Polyakov loop can only be achieved if the configurations are flipped to the real sector with respect to the averaged Polyakov loop.

Then – in the confining phase – the pattern of the Polyakov loop, found inside single clusters (“dyons”) of the topological charge densities  $q_{i,N}(x)$ , reflects with high precision the respective fermionic temporal boundary condition of type  $i$ , that has been applied when the low-lying overlap spectrum was determined. For dyons within a caloron solution, their monopole property *strictly requires* that the monopole centers are populating the sides of the Polyakov triangle. The study of the distribution of the local Polyakov loop values requires an appropriate number of over-improved cooling steps that has been well-defined for the confinement phase.

Just above the transition, cooling strongly influences the averaged Polyakov loop as well as the local Polyakov loop inside the topological clusters towards the trivial corners of the Polyakov triangle (irrespective of the boundary conditions used to find the clusters).



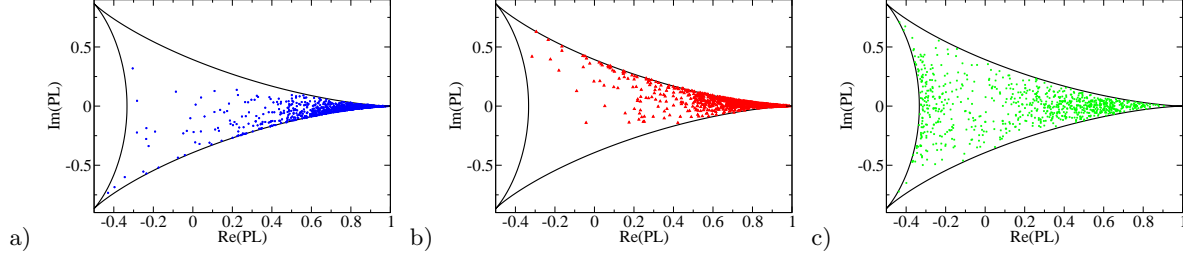


FIG. 7: The same as in Fig. 5 but for the ensemble at  $\beta = 8.25$  ( $T \gtrsim T_c$ ). a) 1036 clusters of first light type (blue), b) 1032 clusters of second light type (red), c) 858 clusters of heavy type (green).

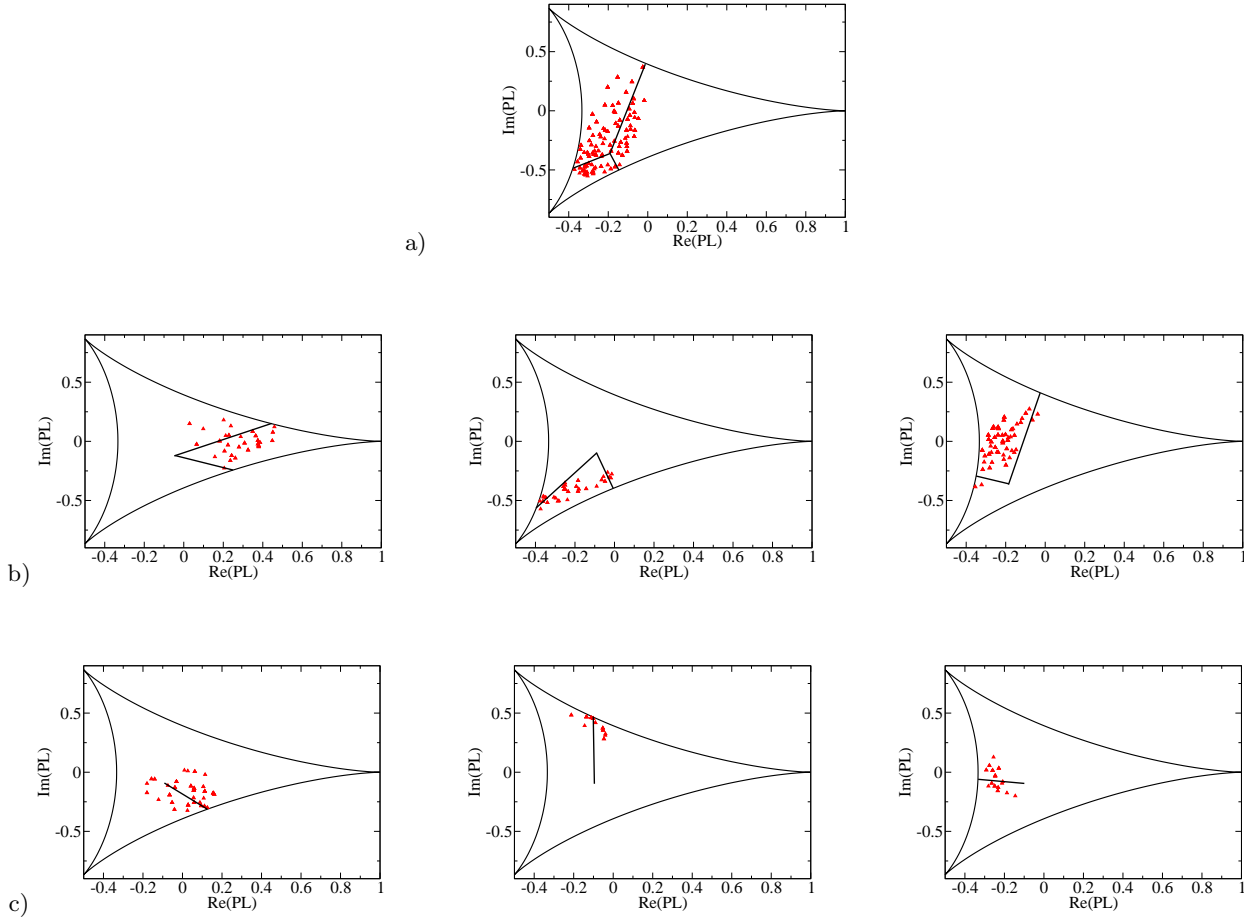


FIG. 8: The profile of the local Polyakov loop  $PL$  in examples of topological “clouds” formed a) by a triplet of clusters (top), b) by (three types of) cluster pairs (middle) and c) consisting of (three types of) isolated clusters (bottom). The pattern obtained for  $\beta = 8.20$  is characteristic for the confining phase. In the figures straight lines are connecting the point representing the averaged Polyakov loop  $L$  of the cooled configuration and the point(s) representing the local Polyakov loop  $PL$  in the respective dyon center(s).

If – in the confining phase – clusters of different type appear correlated (in pairs or triples) or isolated, then the Polyakov loop distribution inside the topological

charge “clouds” corresponds to what is expected from the classical caloron solutions.

Finally we can conclude that we have confirmed the

appearance of topological objects like KvBLL calorons and their dyon constituents in the confined phase of finite temperature  $SU(3)$  Yang-Mills theory at an intermediate resolution scale. This is very similar to what we found earlier in the  $SU(2)$  case [19, 20, 22]. In the deconfinement phase dominance of light dyon constituents was seen, whereas the interpretation of the “heavy” clusters found with antiperiodic boundary conditions did not turn out to be fully conclusive.

In as far the calorons and/or their constituents really may play a major role in the path integral representation for the partition function and for providing e.g. confinement for static quarks can only be seen by model calculations like those carried out for the  $SU(2)$  case [11–13]. Moreover, it remains to be seen, how this picture becomes modified in the presence of dynamical fermions, i.e. in full QCD.

### Acknowledgments

B.V.M. appreciates the support of Humboldt University Berlin where the main part of the work was finalized. We thank F. Bruckmann for careful reading of the manuscript and some hints to improve it.

### Appendix: $SU(3)$ calorons

For completeness and better understanding we recall some facts (from Ref. [37]) and add some more details about calorons and their dyon constituents. The  $SU(N)$  instantons at finite temperature (or calorons) with non-trivial holonomy [6–8] can be considered as composites of  $N$  constituent monopoles, seen only when the Polyakov loop at spatial infinity (holonomy) is non-trivial. In the periodic gauge,  $A_\mu(t + \beta, \vec{x}) = A_\mu(t, \vec{x})$  it is defined as

$$\mathcal{P}_\infty = \lim_{|\vec{x}| \rightarrow \infty} P \exp\left(\int_0^\beta A_0(\vec{x}, t) dt\right). \quad (7)$$

After a suitable constant gauge transformation, the Polyakov loop can be characterised by real numbers  $\mu_{m=1, \dots, n}$  ( $\sum_{m=1}^n \mu_m = 0$ ) that describe the eigenvalues of the holonomy

$$\mathcal{P}_\infty^0 = \exp[2\pi i \text{diag}(\mu_1, \dots, \mu_n)], \quad (8)$$

$$\mu_1 \leq \dots \leq \mu_n \leq \mu_{n+1} \equiv 1 + \mu_1.$$

In units, where the inverse temperature  $\beta = 1$ , a simple formula for the  $SU(N)$  action density can be written [6, 7] :

$$\begin{aligned} \text{Tr} F_{\mu\nu}^2(x) &= \partial_\mu^2 \partial_\nu^2 \log \psi(x), \\ \psi(x) &= \frac{1}{2} \text{tr}(\mathcal{A}_n \cdots \mathcal{A}_1) - \cos(2\pi t), \\ \mathcal{A}_m &\equiv \frac{1}{r_m} \begin{pmatrix} r_m & |\vec{y}_m - \vec{y}_{m+1}| \\ 0 & r_{m+1} \end{pmatrix} \begin{pmatrix} c_m & s_m \\ s_m & c_m \end{pmatrix}, \end{aligned} \quad (9)$$

with  $r_m = |\vec{x} - \vec{y}_m|$  and  $\vec{y}_m$  being the center of mass radii of  $m$  constituent monopoles, which can be assigned a mass  $8\pi^2 \nu_m$ , where  $\nu_m \equiv \mu_{m+1} - \mu_m$ . Furthermore,  $c_m \equiv \cosh(2\pi \nu_m r_m)$ ,  $s_m \equiv \sinh(2\pi \nu_m r_m)$ ,  $r_{n+1} \equiv r_1$  and  $\vec{y}_{n+1} \equiv \vec{y}_1$ .

For  $SU(3)$  calorons we correspondingly parametrize the asymptotic holonomy as  $\mathcal{P}_\infty^0 = \text{diag}(e^{2\pi i \mu_1}, e^{2\pi i \mu_2}, e^{2\pi i \mu_3})$ , with  $\mu_1 \leq \mu_2 \leq \mu_3 \leq \mu_4 = 1 + \mu_1$  and  $\mu_1 + \mu_2 + \mu_3 = 0$ . Let  $\vec{y}_1, \vec{y}_2$  and  $\vec{y}_3$  be three 3D position vectors of dyons remote from each other. Then a caloron consists of three lumps carrying the instanton action split into fractions  $m_1 = \mu_2 - \mu_1$ ,  $m_2 = \mu_3 - \mu_2$  and  $m_3 = \mu_4 - \mu_3$ , concentrated near the  $\vec{y}_i$ .

Provided the constituents are well separated, the local holonomies at the constituents' positions  $\vec{y}_m$ ,  $m = 1, 2, 3$  are [42]

$$\begin{aligned} \mathcal{P}(\vec{y}_1) &= \text{diag}(e^{-\pi i \mu_3}, e^{-\pi i \mu_3}, e^{2\pi i \mu_3}), \\ \mathcal{P}(\vec{y}_2) &= \text{diag}(e^{2\pi i \mu_1}, e^{-\pi i \mu_1}, e^{-\pi i \mu_1}), \\ \mathcal{P}(\vec{y}_3) &= \text{diag}(-e^{-\pi i \mu_2}, e^{2\pi i \mu_2}, -e^{-\pi i \mu_2}). \end{aligned} \quad (10)$$

The complex numbers representing the trace of the holonomy, i.e. the Polyakov loop  $PL = \frac{1}{3} \text{Tr} \mathcal{P}$ , occupy some region on the complex plane. The particular holonomies in Eq. (10) (with twofold degenerate eigenvalues) would guarantee that the local Polyakov loops at the constituents' positions fall onto the boundary of the complex domain (see Figs. 5, 6, and 7).

The trace of the holonomy  $\mathcal{P}_\infty^0$  is three times the Polyakov loop  $PL_\infty$  close to the spatial average of the Polyakov loop  $L$ , which is vanishing in the confining phase and deviating from zero in the deconfining phase.

There is a one-to-one correspondence between the complex Polyakov loop and three real numbers (fractions)  $m_1, m_2, m_3, m_1 + m_2 + m_3 = 1$  that are defined by the eigenvalues of  $SU(3)$  matrix and hence by its trace. Three such numbers can be represented by the inner point of an equilateral triangle for which the sum of the lengths of the three perpendiculars to the triangle sides is constant (equal to one, see Fig. 9). The domain in the complex plane occupied by the Polyakov loop can be considered as some nonlinear deformation of this equilateral triangle. The point  $O$  on Fig. 9 corresponds to  $PL_\infty$ , while the points  $A_1, A_2, A_3$  correspond to the values of the local Polyakov loop at the constituent positions (10). The fermion zero mode  $\psi$  in the background of a KvBLL solution was found [15, 16] for arbitrary temporal boundary conditions  $\psi(t + 1/T, \vec{x}) = \exp(i\phi)\psi(t, \vec{x})$ . The exciting property of the zero mode is that it locates on only one of the dyons. In particular it is located on the  $m$ -th dyon when  $\phi/(2\pi) \in \{\mu_m, \mu_{m+1}\}$ .

For the case of maximally nontrivial holonomy expected to be realized deeply in the confinement phase we have degenerate masses  $m_1 = m_2 = m_3 = 1/3$  and  $\mu_1 = -1/3, \mu_2 = 0, \mu_3 = 1/3$ . Therefore, when

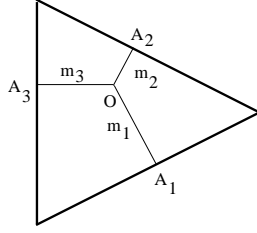


FIG. 9: The equilateral triangle with an inner point  $O$  and three perpendicular projections to the triangle sides. The sum of them  $OA_1 + OA_2 + OA_3 \equiv m_1 + m_2 + m_3 = 1$  is constant for all inner points.

$\phi/(2\pi) \in \{-1/3, 0\}$ , the zero mode is located on the first dyon and for  $\phi = \phi_1 = -\pi/3$  its localization is maximal. For  $\phi = \phi_2 = \pi/3$  and  $\phi = \phi_3 = \pi$  it is maximal on the second and third dyon, respectively.

On the contrary, for the limiting case of maximally trivial holonomy with  $\mu_1 = \mu_2 = \mu_3 = 0$  (i.e.  $PL_\infty =$

$+1$ ) – realized for the real  $Z(3)$  Polyakov loop sector deeply in the deconfinement phase – we obtain asymmetric constituent masses as  $m_1 = m_2 = 0, m_3 = 1$ . The localization of the only massive constituent is then observed with the zero mode related to the antiperiodic boundary condition ( $\phi = \phi_3 = \pi$ ).

- 
- [1] M. Lüscher, JHEP **1008**, 071 (2010), 1006.4518.
  - [2] M. Lüscher (2013), 1308.5598.
  - [3] M. Garcia Perez, O. Philipsen, and I.-O. Stamatescu, Nucl. Phys. **B551**, 293 (1999), hep-lat/9812006.
  - [4] T. Schäfer and E. V. Shuryak, Rev. Mod. Phys. **70**, 323 (1998), hep-ph/9610451.
  - [5] D. Diakonov, Prog. Part. Nucl. Phys. **51**, 173 (2003), hep-ph/0212026.
  - [6] T. C. Kraan and P. van Baal, Nucl.Phys. **B533**, 627 (1998), hep-th/9805168.
  - [7] T. C. Kraan and P. van Baal, Phys.Lett. **B435**, 389 (1998), hep-th/9806034.
  - [8] K.-M. Lee and C.-H. Lu, Phys.Rev. **D58**, 025011 (1998), hep-th/9802108.
  - [9] A. M. Polyakov, Nucl. Phys. **B120**, 429 (1977).
  - [10] B. Martemyanov and S. Molodtsov, JETP Lett. **65**, 142 (1997).
  - [11] P. Gerhold, E.-M. Ilgenfritz, and M. Müller-Preussker, Nucl. Phys. **B760**, 1 (2007), hep-ph/0607315.
  - [12] D. Diakonov and V. Petrov, Phys.Rev. **D76**, 056001 (2007), 0704.3181.
  - [13] F. Bruckmann, S. Dinter, E.-M. Ilgenfritz, B. Maier, M. Müller-Preussker, and M. Wagner, Phys.Rev. **D85**, 034502 (2012), 1111.3158.
  - [14] E.-M. Ilgenfritz, K. Koller, Y. Koma, G. Schierholz, T. Streuer, and V. Weinberg, Phys.Rev. **D76**, 034506 (2007), 0705.0018.
  - [15] M. Garcia Perez, A. Gonzalez-Arroyo, C. Pena, and P. van Baal, Phys.Rev. **D60**, 031901 (1999), hep-th/9905016.
  - [16] M. N. Chernodub, T. C. Kraan, and P. van Baal, Nucl. Phys. Proc. Suppl. **83**, 556 (2000), hep-lat/9907001.
  - [17] C. Gattringer, Phys. Rev. **D67**, 034507 (2003), hep-lat/0210001.
  - [18] C. Gattringer and S. Schaefer, Nucl. Phys. **B654**, 30 (2003), hep-lat/0212029.
  - [19] V. Bornyakov, E.-M. Ilgenfritz, B. Martemyanov, S. Morozov, M. Müller-Preussker, and A. Veselov, Phys.Rev. **D76**, 054505 (2007), 0706.4206.
  - [20] V. Bornyakov, E.-M. Ilgenfritz, B. Martemyanov, and M. Müller-Preussker, Phys.Rev. **D79**, 034506 (2009), 0809.2142.
  - [21] E. M. Ilgenfritz, M. Müller-Preussker, and D. Peschka, Phys.Rev. **D71**, 116003 (2005), hep-lat/0503020.
  - [22] E.-M. Ilgenfritz, B. Martemyanov, M. Müller-Preussker, and A. Veselov, Phys.Rev. **D73**, 094509 (2006), hep-lat/0602002.
  - [23] E.-M. Ilgenfritz, B. Martemyanov, M. Müller-Preussker, and A. Veselov, Phys.Rev. **D71**, 034505 (2005), hep-lat/0412028.
  - [24] M. Lüscher and P. Weisz, Commun.Math.Phys. **97**, 59 (1985).
  - [25] C. Gattringer, R. Hoffmann, and S. Schaefer, Phys.Rev. **D65**, 094503 (2002), hep-lat/0112024.
  - [26] C. Gattringer, M. Göckeler, P. Rakow, S. Schaefer, and A. Schäfer, Nucl.Phys. **B618**, 205 (2001), hep-lat/0105023.
  - [27] V. Bornyakov, E. Lushevskaya, S. Morozov, M. Polikarpov, E.-M. Ilgenfritz, and M. Müller-Preussker, Phys.Rev. **D79**, 054505 (2009), 0807.1980.
  - [28] M. Lüscher and P. Weisz, Phys.Lett. **B158**, 250 (1985).
  - [29] J. R. Snippe, Nucl.Phys. **B498**, 347 (1997), hep-lat/9701002.
  - [30] G. P. Lepage and P. B. Mackenzie, Phys.Rev. **D48**, 2250 (1993), hep-lat/9209022.
  - [31] C. Gattringer, R. Hoffmann, and S. Schaefer, Phys.Lett. **B535**, 358 (2002), hep-lat/0203013.
  - [32] C. Gattringer, P. E. L. Rakow, A. Schäfer, and W. Söldner, Phys. Rev. **D66**, 054502 (2002), hep-lat/0202009.
  - [33] P. Hasenfratz, V. Laliena, and F. Niedermayer, Phys. Lett. **B427**, 125 (1998), hep-lat/9801021.
  - [34] C. Aubin et al. (MILC), Nucl. Phys. Proc. Suppl. **140**, 626 (2005), hep-lat/0410024.

- [35] M. I. Polikarpov, F. V. Gubarev, S. M. Morozov, and V. I. Zakharov, PoS **LAT2005**, 143 (2006), hep-lat/0510098.
- [36] M. Garcia Perez, A. Gonzalez-Arroyo, J. R. Snippe, and P. van Baal, Nucl.Phys. **B413**, 535 (1994), hep-lat/9309009.
- [37] V. Bornyakov, E.-M. Ilgenfritz, B. Martemyanov, V. Mitrjushkin, and M. Müller-Preussker, Phys.Rev. **D87**, 114508 (2013), 1304.0935.
- [38] C. Gattringer, E. M. Ilgenfritz, and S. Solbrig (2006), hep-lat/0601015.
- [39] F. Bruckmann, C. Gattringer, E.-M. Ilgenfritz, M. Müller-Preussker, A. Schäfer, and S. Solbrig, Eur.Phys.J. **A33**, 333 (2007), hep-lat/0612024.
- [40] F. Bruckmann, F. Gruber, C. Lang, M. Limmer, T. Maurer, A. Schäfer, and S. Solbrig, PoS **CONFINEMENT8**, 045 (2008), 0901.2286.
- [41] C. Gattringer, E.-M. Ilgenfritz, B. V. Martemyanov, M. Müller-Preussker, D. Peschka, R. Pullirsch, S. Schaefer, and A. Schäfer, Nucl.Phys.Proc.Suppl. **129**, 653 (2004), hep-lat/0309106.
- [42] P. van Baal, Proceedings *Lattice fermions and structure of the vacuum*, JINR Dubna, pp. 269–279 (1999), hep-th/9912035.
- [43] E.-M. Ilgenfritz, D. Leinweber, P. Moran, K. Koller, G. Schierholz, et al., Phys.Rev. **D77**, 074502 (2008), 0801.1725.
- [44] The idea to confront the filtering provided by a given cut-off in analyzing modes with the filtering effected by cooling was also the guiding idea of Ref. [43]. Extended to  $O(50)$  cooling steps and matching to the corresponding cut applied to the overlap modes, both techniques agreed on the existence of bigger topological lumps with instanton properties. The search for constituents was not within the scope of that paper.